Chemistry & Biology, Vol. 11, 1179–1194, September, 2004, ©2004 Elsevier Ltd. All rights reserved. DOI 10.1016/j.chembiol.2004.05.024

# An Aldol Switch Discovered in Stilbene Synthases Mediates Cyclization Specificity of Type III Polyketide Synthases

**Michael B. Austin,[1,2] Marianne E. Bowman,[1] Jean-Luc Ferrer,[3] Joachim Schröder,[4] and Joseph P. Noel[1,2,*]**

[1]Structural Biology Laboratory
The Salk Institute for Biological Studies
10010 North Torrey Pines Road
La Jolla, California 92037

[2]Department of Chemistry and Biochemistry
University of California, San Diego
La Jolla, California 92037

[3]IBS J.-P. Ebel
41 rue Jules Horowitz
38027 Grenoble Cedex 1
France

[4]Institut für Biologie II
Biochemie der Pflanzen
Universität Freiburg
Schänzlestrasse 1
D-79104 Freiburg
Germany

## Summary

**Stilbene synthase (STS) and chalcone synthase (CHS) each catalyze the formation of a tetraketide intermediate from a CoA-tethered phenylpropanoid starter and three molecules of malonyl-CoA, but use different cyclization mechanisms to produce distinct chemical scaffolds for a variety of plant natural products. Here we present the first STS crystal structure and identify, by mutagenic conversion of alfalfa CHS into a functional stilbene synthase, the structural basis for the evolution of STS cyclization specificity in type III polyketide synthase (PKS) enzymes. Additional mutagenesis and enzymatic characterization confirms that electronic effects rather than steric factors balance competing cyclization specificities in CHS and STS. Finally, we discuss the problematic in vitro reconstitution of plant stilbenecarboxylate pathways, using insights from existing biomimetic polyketide cyclization studies to generate a novel mechanistic hypothesis to explain stilbenecarboxylate biosynthesis.**

## Introduction

Type III polyketide synthases (PKSs) are structurally simple, homodimeric iterative PKSs (Figure 1A) that utilize a conserved Cys-His-Asn catalytic triad in an internal active site (Figure 1B) to catalyze the iterative condensation of acetyl units (derived from malonyl-CoA) to a CoA-linked starter molecule (Figure 1C). This chain extension is usually followed by cyclization of the linear polyketide intermediate in the same active site cavity [1, 2]. The more than a dozen functionally distinct plant and bacterial type III PKS enzyme families characterized to date differ in their choice of CoA-tethered starter molecule, in the number of polyketide elongation steps catalyzed, and in the mechanism for intramolecular cyclization of linear polyketide intermediates, thereby producing a variety of biologically and medicinally important natural product classes [2]. While the enzymatic features that mediate starter molecule selection and polyketide chain extension are largely understood, type III PKS control of cyclization specificity remains a mystery.

The classic illustration of this latter point contrasts the first two examples of type III PKS to be discovered: the chalcone synthase (CHS) and stilbene synthase (STS) enzyme families [3]. STS has independently evolved in a few diverse plants (such as grapevine, pine, and peanut) via the duplication and divergence of *chs* genes, the latter of which are ubiquitous in higher plants [4]. Despite their limited occurrence in nature, the di- and trihydroxylated stilbene scaffolds produced by STS have recently received much attention due to their numerous biological activities. Expression of *sts* genes confers significant resistance against fungal infection to both natural and heterologous host plants [5, 6]. Resveratrol (trihydroxy-stilbene) is also believed to be a major contributor to the health benefits associated with the moderate consumption of red wine (known as "the French paradox") [7]. Indeed, animal cell culture studies have linked an impressive number of beneficial medicinal effects to resveratrol and other stilbenes, including copper chelation, antioxidant scavenging of free radicals, inhibition of both platelet aggregation and lipid peroxidation, antiinflammatory activity, vasodilation, and anticancer activities [8, 9]. Most recently, resveratrol was found to delay apoptosis through a 13-fold stimulation of the sirtuin-family deacetylase activity that negatively regulates the p53 tumor suppressor, resulting in the same significant extension of organismal lifespan previously observed in connection with severe restriction of caloric intake [10].

CHS and STS enzymes share 75%–90% amino acid sequence identity over their ~400 residues, and both enzyme families catalyze the same iterative condensation of three acetyl units (derived from the decarboxylation of malonyl-CoA) to a CoA-tethered phenylpropanoid starter molecule (derived from phenylalanine), most typically *p*-coumaroyl-CoA. However, STS enzymes cyclize the resulting tetraketide intermediate product via an intramolecular C2→C7 aldol condensation, rather than the intramolecular C6→C1 Claisen condensation utilized by CHSs (Figure 1D) [11].

Previously, the alfalfa CHS crystal structure implied that proper orientation of CHS's enzyme-bound tetraketide intermediate by residues lining the internal active site cavity is sufficient to promote the CHS intramolecular Claisen cyclization reaction [12]. This C6→C1 cyclization also conveniently results in cleavage of the C1 thioester linkage to the CHS enzyme, thus offloading the chalcone product. Conversely, the STS C2→C7 reaction requires a thioesterase-like hydrolysis step to cleave the C1 thioester linkage to the STS enzyme, as well as

*Correspondence: noel@salk.edu

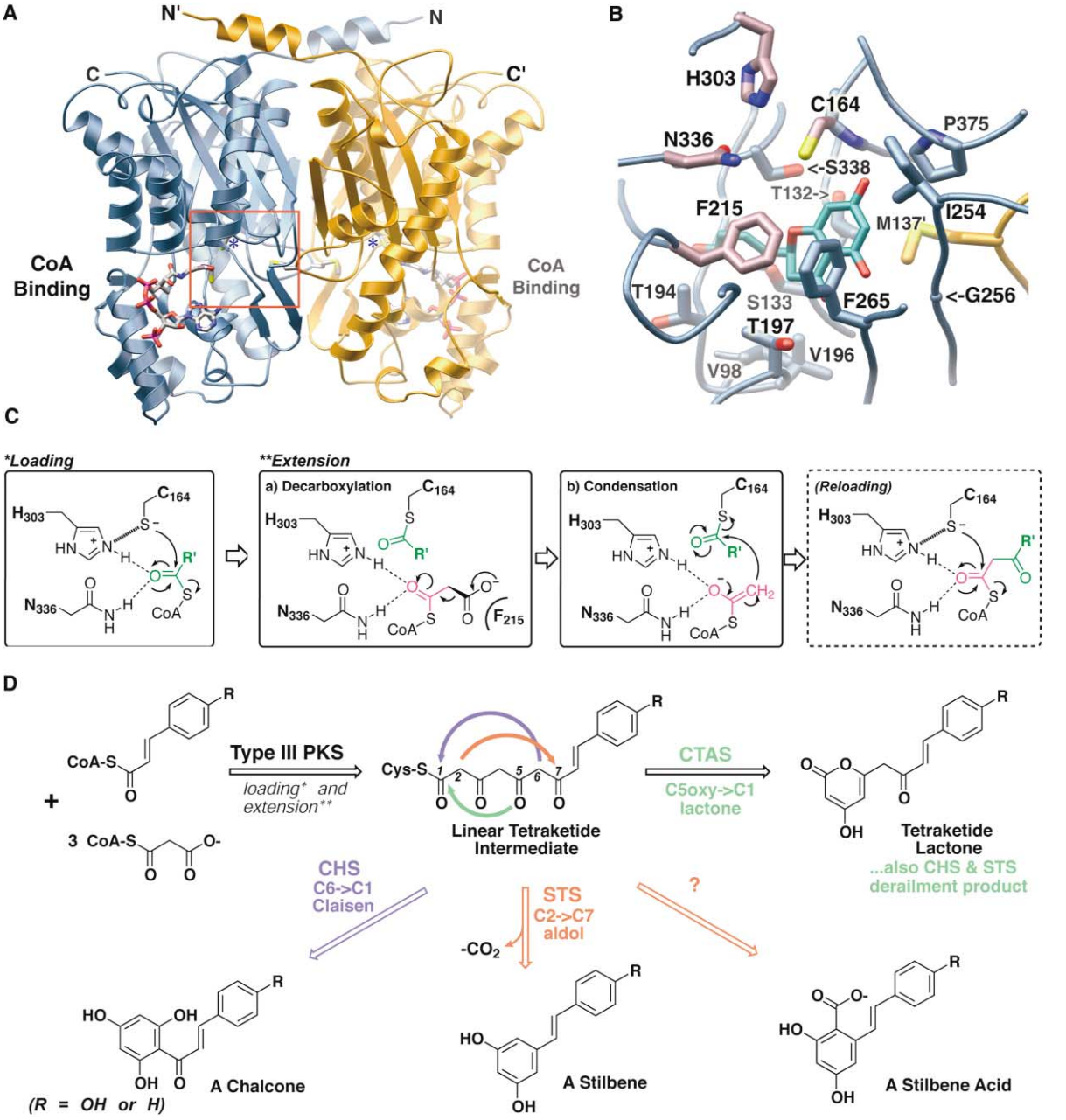


Figure 1. Type III Polyketide Synthase Enzymes and Tetraketide Cyclization

(A) Type III PKS homodimeric architecture (blue and gold) and CoA binding based upon alfalfa chalcone synthase (CHS) crystal structures [12]. Bound CoA (stick model) highlights the entrance to the CoA binding tunnel for each monomer's internal active site cavity (red box: see [B]). Catalytic cysteine positions are noted (blue asterisks).

(B) CHS active site cavity occupied by chalcone-derived naringenin (cyan), shown from the perspective of the CoA binding tunnel. Shown are the condensing machinery (Cys-His-Asn catalytic triad and Phe215) in rose, additional residues lining the active site cavity (blue), and the only active site cavity residue contributed by the dyad-related monomer (gold).

(C) Type III PKS condensing mechanism (starter loading and polyketide extension). CoA-linked starter moieties (green) are covalently loaded onto the catalytic cysteine. The decarboxylation of malonyl-CoA produces an activated acetyl unit (pink) that undergoes Claisen condensation with the cysteine-bound starter moiety. The resulting diketide intermediate is transferred from CoA to the catalytic cysteine for additional two-carbon extension reactions.

(D) Identical tetraketide intermediates produced by CHS and STS (stilbene synthase) reactions, from *p*-coumaroyl-CoA (R = OH) or cinnamoyl-CoA (R = H) starter molecules. This tetraketide intermediate initially forms as a CoA-thioester, rather than the enzyme-linked thioester depicted here. Alternative intramolecular cyclization patterns lead to different natural product scaffolds. The blue arrow depicts CHS's C6→C1 Claisen condensation leading to hydroxylated chalcones, the red arrow shows the C2→C7 aldol condensation leading to the STS-synthesized hydroxylated stilbenes discussed here (resveratrol [R = OH] and pinosylvin [R = H]), and the green arrow illustrates the C5-oxygen→C1 lactonization associated with *p*-coumaroyl tetraacetic acid synthase (CTAS, see text), as well as product derailment in both CHS and STS. Finally, the still unresolved reaction leading to stilbene acids is depicted.

Table 1. Crystallographic Data and Refinement Statistics

| | STS | 18xCHS | 18xCHS + Resveratrol |
|---|---|---|---|
| Space group | P2(1) | P2(1) | P1 |
| Unit cell dimensions (Å,°) | a = 57.2, b = 361.3, c = 57.3, β = 98.4 | a = 71.6, b = 59.8, c = 82.5, β = 108.2 | a = 64.3, b = 71.7, c = 85.7, α = 111.4, β = 91.6, γ = 90.1 |
| Wavelength (Å) | 0.933 | 0.931 | 0.773 |
| Resolution (Å) | 2.1 | 1.9 | 2.0 |
| Total reflections | 202,864 | 186,828 | 189,393 |
| Unique reflections | 103,258 | 52,432 | 93,036 |
| Completeness[a] (%) | 74.1 (34.1) | 98.7 (99.9) | 97.5 (96.8) |
| $I/\sigma$[a] | 4.2 (1.6) | 13.6 (3.8) | 14.1 (2.2) |
| $R_{sym}$[a,b] | 18.2 (30.7) | 4.4 (17.0) | 5.8 (30.4) |
| $R_{cryst}$[c]/$R_{free}$[d] (%) | 22.5/28.9 | 19.3/23.0 | 20.3/26.4 |
| Protein atoms | 17,892 | 5,881 | 11,896 |
| Ligand atoms | — | — | 69 |
| Water molecules | 1871 | 716 | 1190 |
| Rmsd bond lengths (Å) | 0.008 | 0.006 | 0.010 |
| Rmsd bond angles (°) | 1.4 | 1.3 | 1.5 |
| Average B factor: protein (Å$^2$) | 34.9 | 20.4 | 31.1 |
| Average B factor: solvent (Å$^2$) | 69.0 | 67.0 | 51.0 |

[a] Number in parenthesis is for the highest resolution shell.
[b] $R_{sym} = \Sigma|I_h - \langle I_h \rangle|/\Sigma I_h$, where $\langle I_h \rangle$ is the average intensity over symmetry equivalent reflections.
[c] R factor = $\Sigma||F_{obs}| - |F_{calc}||/\Sigma|F_{obs}|$, where summation is over the data used for refinement.
[d] $R_{free}$ factor is the same definition as for R factor, but includes only 5% of data excluded from refinement.

an additional decarboxylative elimination of the resulting C1 carboxylate. However, sequence comparison of the STS subfamilies both to each other and to CHS reveals no apparent STS consensus sequence [4], and homology modeling carried out in our lab on STS enzymes subsequent to determination of the alfalfa CHS2 crystal structure predicted no significant topological or chemical differences in the STS active site cavities relative to CHS.

In the absence of any convincing STS sequence-related or structural evidence, it has been presumed that some steric reshaping of the active site cavity, relative to CHS, directs the divergent C2→C7 aldol cyclization specificity of STS. While this steric modulation hypothesis provides a reasonable explanation for how STS could achieve an alternative productively folded conformation of the linear tetraketide intermediate it shares with CHS [12, 13], this model fails to account for the additional STS thioesterase activity and polyketide C1 decarboxylation steps required for biosynthesis of the stilbene scaffold. Notably, no structural feature of STS related to catalysis of the thioesterase activity has yet been identified or even proposed. The timing and mechanistic relevance of the C1 decarboxylation step also remains unresolved, although this process was recently determined to occur prior to aromatization of the stilbene product's newly formed dihydroxyphenyl ring moiety [14].

To illuminate the structural and mechanistic basis for the intramolecular aldol cyclization specificity of STS enzymes, we here present our structural elucidation of a pinosylvin-forming STS from *Pinus sylvestris* (Scots pine) [15]. This first stilbene synthase crystal structure disfavors the prevailing model that STS achieves aldol cyclization specificity through steric modulation of the active site architecture and instead implicates an unanticipated chemical mechanism guided by the emergence of a cryptic thioesterase activity. Our subsequent structure-guided mutagenic conversion of alfalfa CHS into a functional stilbene synthase confirms our identification of the "aldol switch" structural changes responsible for aldol cyclization specificity. Further subtle mutations designed to perturb only the proposed thioesterase step support our conclusions. Finally, we offer a novel mechanistic proposal for the biosynthesis of stilbenecarboxylic acids that draws circumstantial support from a number of biomimetic polyketide cyclization studies.

## Results and Discussion

### 2.1 Å Crystal Structure of Pinosylvin-Forming Stilbene Synthase from *P. sylvestris*

The unusual length (361.3 Å) of one of the crystallographic axes of the pine STS unit cell translates into reflections that are closely spaced and overlapped. Deconvolution of these overlaps represented a significant data processing obstacle, similar to problems encountered in crystallographic analyses of virus structures, that here impacts both the completeness and quality of even our best pine STS data set (see Experimental Procedures and Table 1). However, despite poorer statistics relative to most structures of similar resolution, even the initial STS $2F_o - F_c$ and $F_o - F_c$ electron density difference maps were highly informative, clearly showing the structural differences between STS and the initial CHS-derived STS homology model. Moreover, the structural and mechanistic conclusions gleaned from this first STS crystal structure were independently verified by the mutagenic conversion of polyketide cyclization specificity achieved in STS structure-guided CHS mutants. The higher statistical quality of the subsequent apo and resveratrol-complexed crystal structures of one such mutant enzyme (detailed below and in Table 1) further validates the value and accuracy of the pine STS crystal structure.

As expected, Scots pine STS closely adheres to the

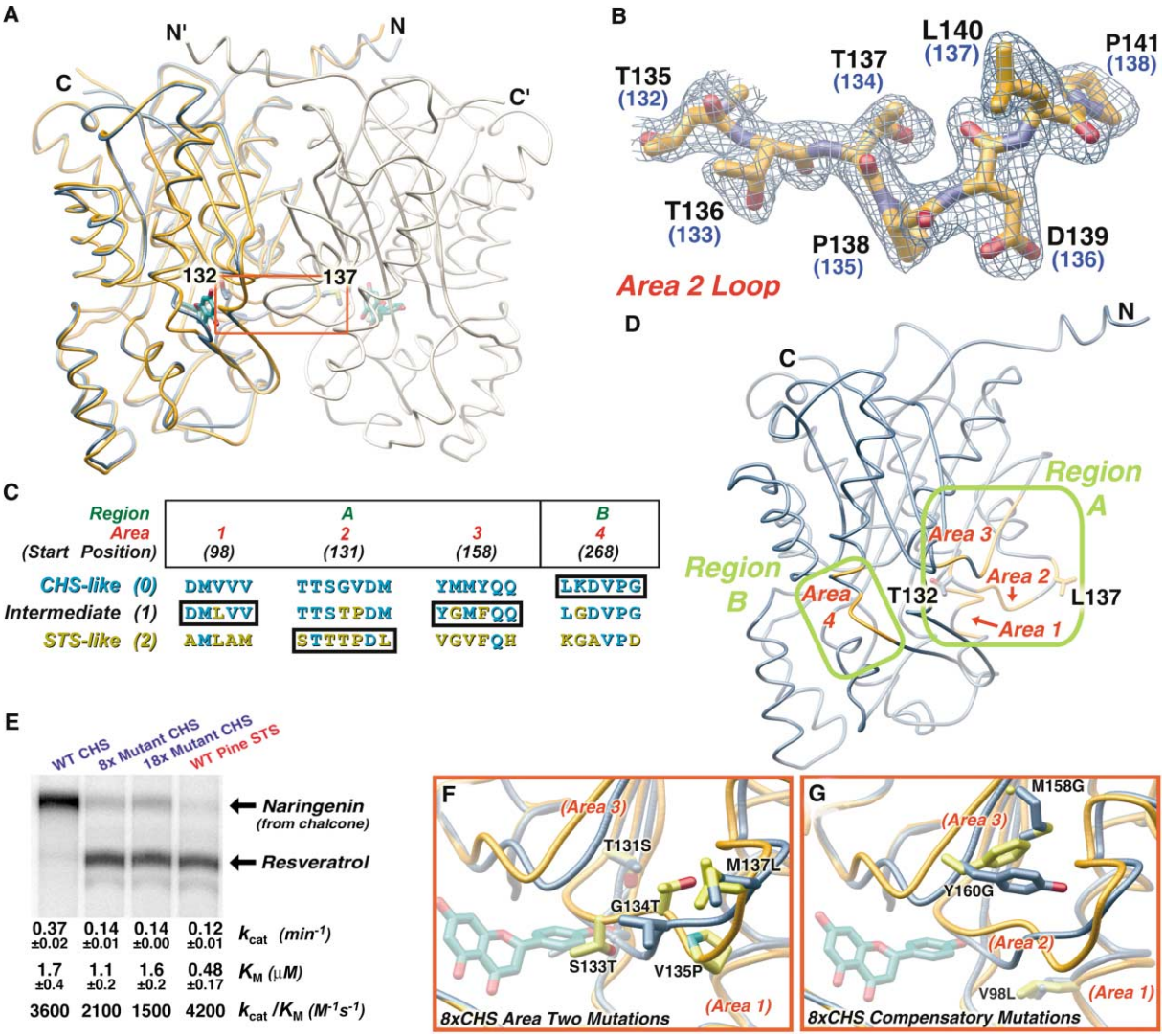


Figure 2. STS Crystal Structures and Functionally Relevant Differences

(A) C-α trace of one monomer (gold) of the homodimeric pine STS 2.1 Å crystal structure overlaid with the alfalfa CHS homodimer (gray and blue), shown here with naringenin bound in each CHS active site cavity. A red box highlights the area 2 loop that separates these juxtaposed active site cavities. CHS residues 132 and 137, which contribute to dyad-related active site cavities, are also shown.

(B) Close-up view of the conformationally divergent pine STS area 2 loop (with equivalent CHS numbering in blue), showing the final $2F_o - F_c$ electron density map (blue wirecage) contoured at 1 sigma.

(C) Alignment table defining CHS-like, intermediate, or STS-like (respectively labeled 0, 1, or 2; see text for explanation) sequences in region A (areas 1–3) and region B (area 4). The intermediate sequences represent our initial guesses of the functionally relevant differences between the two wild-type sequences, and are also the mutations introduced in the first of two rounds of mutagenesis necessary to fully convert each relevant area in CHS to the STS-like sequence (see Experimental Procedures). CHS residues (unique or shared) are blue, while mutations corresponding to the pine STS sequence are gold. Gold residues in the bottom row correspond to the 18 mutations comprising the 18xCHS (2222) alfalfa CHS mutant that functions as an authentic STS. Gold residues in the black boxes comprise the eight mutations in the STS-like 8xCHS (1210) mutant.

(D) C-α trace of the 1.9 Å crystal structure of the resveratrol-producing 18xCHS mutant. Mutated positions corresponding to region A (areas 1–3) and region B (area 4) are in gold. Side chains of positions 132 and 137 are shown for clarity.

(E) Resveratrol-forming cyclization specificity of engineered stilbene synthases (8xCHS and 18xCHS), compared to the observed product specificity of wild-type alfalfa CHS and pine STS enzymes, illustrated using a thin layer chromatography (TLC) analysis of identical reactions using *p*-coumaroyl-CoA as starter molecule. (CHS's enzymatic chalcone product undergoes a facile Michael addition reaction in solution to form the flavanone naringenin.) Steady-state kinetic constants for each reaction (see text) are tabulated below. Units of $k_{cat}$, $K_M$, and $k_{cat}/K_M$ are $min^{-1}$, μM, and $M^{-1}s^{-1}$, respectively. Average values are shown (n = 3).

(F) Five 8xCHS area 2 loop mutations shown on an overlay of wild-type alfalfa CHS (blue) and wild-type pine STS (gold) structures.

(G) Three 8xCHS areas 1 and 3 compensatory mutations shown in overlay of wild-type CHS (blue) and wild-type STS (gold) structures.

same overall structural fold observed in the two previously structurally characterized plant type III PKSs [12, 16]. The αβαβα core of this fold, also known as the thiolase fold, is conserved among all thiolase and condensing enzymes crystallized to date, exposing their ancient evolutionary relationship [2]. Surprisingly, crys-

tallographic comparison of the pine STS active site cavity to that of alfalfa CHS reveals only very minor differences in topology, none of which seem capable of promoting an alternate conformation of the two enzymes' identical tetraketide intermediate product, as had been theorized [12, 17]. Overall, the C-$\alpha$ trace of the entire STS backbone superimposes almost perfectly with that of CHS (rmsd = 0.65 Å), diverging significantly in only two regions, defined as A and B (Figures 2A–2D). Indeed, a comparison of these two conformationally distinct STS loops to the equivalent loops in the CHS structure reveals a C-$\alpha$ rmsd of 2.0 Å. Notably, these backbone changes are conserved in each of the six noncrystallographically related monomers (three physiological dimers) that comprise the pine STS crystal's unusually large asymmetric unit.

Region A spans a buried 6 residue loop, located at the dimer interface, that separates the two monomers' identical active sites. Thr135 at one end of the loop contributes to the active site of its polypeptide chain while Leu140 at the other end of the loop contributes to the opposing active site cavity (Figures 2A and 2B). In STS, this loop is displaced relative to the corresponding loop in CHS (residues 132–137 in alfalfa CHS), ostensibly due to the presence of proline (Figure 2B) at position 138 of STS (CHS position 135). Closer examination of this buried region reveals compensatory mutations in two other areas of primary sequence that in the folded protein are juxtaposed either below (area 1) or above (area 3) the displaced loop (area 2). These region A differences in the newly solved STS structure did not significantly alter the shape of the cyclization cavity previously identified in alfalfa CHS2 [12].

Conversely, region B is a 3 residue loop (area 4) located on the outer, solvent-exposed surface of the STS CoA binding tunnel (on the rim opposite the CoA phosphate binding residues) (Figure 2D), whose displacement relative to CHS was also observed in the only other type III PKS crystal structure published to date, that of a 2-pyrone synthase (2-PS) from daisy [16]. In 2-PS, this displacement of region B residues toward the pantetheine binding tunnel provides additional hydrogen bonding and van der Waals contacts with bound CoA. We were unable to obtain crystals of the STS-CoA complex. Nevertheless, although the amino acid sequence of region B varies between these two enzymes, it seems probable, as with 2-PS, that displacement of the STS region B loop toward the CoA binding tunnel also causes additional contacts with CoA, principally through the adenine moiety. This arrangement may enhance the on-rate or slow the off-rate of CoA-linked starters, malonyl-CoA extenders, and reactive intermediates. This possible kinetic effect could have mechanistic implications for the balance of competing reactions occurring within the active site cavity.

### Mutagenic Conversions of Alfalfa Chalcone Synthase into Functional Stilbene Synthases

To determine whether any of these crystallographically observed structural differences correlate with the aldol cyclization specificity of STS, we used two rounds of mutagenesis to convert regions A and B (areas 1–4) of alfalfa CHS to the corresponding residues in Scots pine STS (see Figure 2C and Experimental Procedures). Indeed, the resulting 18xCHS mutant functionally resembled wild-type STS, as reflected by both its steady-state kinetic properties and product specificity, producing resveratrol rather than chalcone as the major product of in vitro assays (Figure 2E).

Next, a quasicombinatorial mutagenic PCR strategy using alfalfa CHS as a template was devised to deconvolute the mechanistic contribution toward cyclization specificity of each of the four stretches of primary sequence implicated by the 18xCHS mutant's assay results. In each of these four areas, the alfalfa CHS sequence either remained unchanged (designated by a 0), or was partially (1) or completely (2) mutated to the Scots pine STS sequence (Figure 2C). These CHS mutants were labeled accordingly using a four-digit code to reflect their composition in each area (for example, the 18xCHS mutant was labeled 2222, while wild-type CHS would be labeled 0000). It was neither necessary nor efficient to construct all 81 possible members of this library. Rather, smaller diagnostic sets of mutants were constructed, expressed, purified, and assayed to quickly isolate and identify the mechanistically relevant residues, as outlined below.

This mutagenic approach revealed region B (area 4) to be unimportant for cyclization specificity, but diagnosed region A (areas 1–3, near the dimer interface) as critical for mediating the Claisen to aldol cyclization switch in STS. The product specificity of the area 4 mutant 0002 is identical to wild-type CHS (data not shown), while the activity of the 1210 mutant (8xCHS) closely resembles wild-type STS and the 2222 (18xCHS) mutant (Figure 2E). The 1210 (8xCHS) mutant comprises five changes in the area 2 loop (Figure 2F), as well as one compensatory change in area 1 (below the loop) and two compensatory changes in area 3 (above the loop) (Figure 2G). Unfortunately, nearly all of the more minimal mutants obtained from this library (i.e., combinations 1200, 0210, 1110, 1100, 0110, 1000, 0100, and 0010 from Figure 2C) exhibited very little activity due to protein aggregation and precipitation throughout the expression and purification process. This latter result demonstrates the extent to which the pine STS has structurally reinforced its functionally important area 2 loop conformation since diverging from its CHS ancestor. In the few cases where mutants more minimal than the STS-like 8xCHS were catalytically active, their observed cyclization specificity followed the C6→C1 Claisen condensation route exhibited by wild-type CHS (data not shown). Contrary to expectations, none of the mutant enzymes from this library produced any significant amount of the derailment tetraketide lactone product (pictured in Figure 1D and discussed later) made in trace amounts by both CHS and STS. This lack of significant derailment from the wild-type cyclization pathways indicates a smooth, one-step transition from the C6→C1 Claisen to the C2→C7 aldol condensation mechanism.

### Apo and Resveratrol-Complexed Crystal Structures of Resveratrol-Producing 18xCHS

Two high-resolution structures of the 18xCHS mutant, a functional stilbene synthase, were also determined by

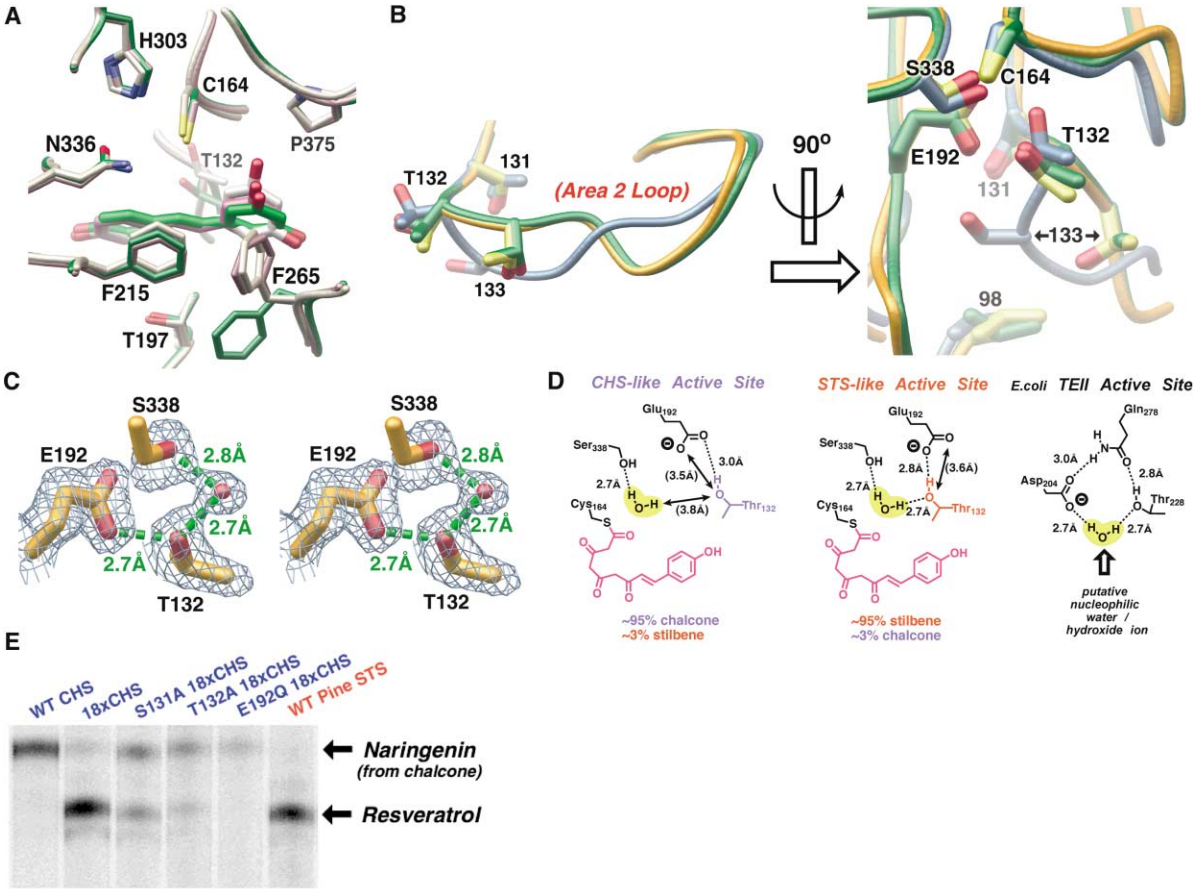


Figure 3. Thioesterase-like STS "Aldol Switch" Controls Cyclization Specificity

(A) Slightly different bound conformations of resveratrol observed in the complexed 18xCHS crystal structure (green and rose) correlate to movements of the flexible Phe265 side chain, overlaid with the structure of the previously determined resveratrol [12] bound in wild-type CHS (light gray) and viewed down the CoA binding tunnel into the active site cavity. Positioning of resveratrol's starter- and malonyl-derived aromatic rings are similar to each other and to CHS-bound naringenin (shown in Figure 1B in a similar view).

(B) C-$\alpha$ trace overlay of the displacement of the area 2 loop in STS (gold) and 18xCHS (green), compared to CHS (blue). Two orientations illustrate the positions and movements of residues 131–133 (CHS numbering).

(C) Stereoview of the 18xCHS STS-like "aldol switch" hydrogen bonds, showing the 1.9 Å resolution $2F_o - F_c$ electron density map (blue wirecage) contoured at 1 sigma.

(D) "Aldol switch" hydrogen bonding differences (resulting from repositioning of the Thr132 side chain) in CHS-like and STS-like active sites, compared to each other and to the active site of thioesterase II (TEII) from *E. coli* ([18]; PDB code 1C8U). Distances incompatible with hydrogen bond formation are given in parentheses and indicated with double-headed arrows. Putative nucleophilic water positions are highlighted in yellow.

(E) Thin layer chromatography (TLC) analysis of the cyclization specificities of mutants designed to disrupt the 18xCHS mutant's aldol switch hydrogen bond network while preserving the 18xCHS STS-like conformational changes (see text).

protein X-ray crystallography, in the apo form (1.9 Å) or with the resveratrol product of STS bound in the active site cavity (2.1 Å) (Table 1). Although a homology model based upon wild-type CHS, rather than STS, was used as the search model for molecular replacement, the initial electron density maps and all subsequent maps revealed STS-like conformational changes in the mutated regions (Figure 2D). Indeed, the conformations of these regions in the alfalfa 18xCHS mutant's area 2 and 4 loop conformations were remarkably STS-like (18xCHS area 2 and 4 loops: C-$\alpha$ rmsd with STS = 0.35 Å, and with CHS = 1.9 Å). However, spotty electron density in the 18xCHS area 4 loop indicates this solvent-exposed loop to be less conformationally restricted in the alfalfa 18xCHS mutant than in wild-type pine STS. No other conformational changes relative to the wild-type CHS structure were observed in the 18xCHS mutant.

Likewise, although the resveratrol-complexed crystal grew in a different space group than the apo 18xCHS crystal (see Table 1), no significant 18xCHS conformational changes occurred upon binding of resveratrol. Moreover, the position and orientation of resveratrol in the active site of this functional stilbene synthase is nearly identical to the positions and orientations of both resveratrol and naringenin (the flavanone resulting from the Michael addition isomerization of the unstable chalcone product) previously observed in wild-type CHS crystal complexes [12] (Figure 3A). This latter result argues against the likelihood of any drastic reorientation within the STS active site cavity, relative to their posi-

tions in CHS, of either the coumaroyl starter molecule or the subsequently formed linear polyketide intermediates common to both enzymes. Two slightly different resveratrol conformations in the four noncrystallographically related monomers of the resveratrol-complexed 18xCHS asymmetric unit (is equal to unit cell for $P_1$ lattice) correlate with positional changes of the relatively disordered Phe265 side chain (Figure 3A). Lack of order and positional differences are typical for this type III PKS "gatekeeper" residue [2, 12], and so the Phe265 differences highlighted in Figure 3A should not be misinterpreted as unique or specific to this complexed structure.

### An Aldol Cyclization Switch in Stilbene Synthase also Constitutes the Missing STS Thioesterase Machinery

We next undertook a closer examination of the region A structural differences implicated as functionally relevant by the 8xCHS mutant's STS-like activity, in order to provide a sound mechanistic hypothesis for STS's aldol cyclization specificity rather than a simple correlative explanation based upon conformational differences. Divergent areas 1 and 3 are completely buried, and only three residues from area 2 contact the type III PKS active site cavity. Residues 132 and 133 (alfalfa CHS numbering) border their own monomers' active site cavity, adjacent to the dyad-related monomer's residue 137 side chain. The 137 position, which is a methionine in alfalfa CHS and a leucine in Scots pine STS, is the only residue in either enzyme that contributes to the active site cavity of the opposing monomer (Figure 1B). Prior to the elucidation of the STS structure, we had exchanged both enzymes' position 137 amino acids based upon homology modeling, but these mutations had no effect on cyclization specificity or catalytic efficiency in either enzyme (data not shown). Conversely, residues 132 and 133 (TT in CHS and TS in STS) were not previously suspected to be important for aldol cyclization specificity, but our comparison of the STS, CHS, and 18xCHS mutant crystal structures reveals an important difference caused by the displacement of the conserved Thr132 residue in the resveratrol-producing enzymes (Figure 3B). While the same buried conformational rearrangement of STS's area 2 loop results in a more drastic lateral displacement of residue 133, it is unlikely that position 133 plays any significant steric or electronic role in the STS cyclization mechanism, due to its more remote location in the active site cavity.

Conversely, the more subtle displacement of Thr132 caused by the buried changes in the area 2 loop brings its side chain hydroxyl moiety within hydrogen bonding distance of a Ser338-stabilized water molecule poised adjacent to the catalytic cysteine (Figures 3C–3D). It should be noted that this active site water molecule is somewhat dynamic, as its position and occupancy can differ in complexes and even between monomers in the same crystal. However, this Ser338-stabilized water molecule is crystallographically observed in the active site cavities of both STS and CHS. In the STS-like active site, the new hydrogen bond to Thr132 electronically connects this water molecule, through the repositioned threonine hydroxyl, to a buried glutamate residue present at the back of all type III PKS active site cavities. This newly identified STS hydrogen bonding configuration is similar, although not identical, to the catalytic machinery of a type II thioesterase recently discovered in *E. coli* [18] (Figure 3D). Significantly, a key difference between the CHS and STS reactions is the need, in STS, for thioesterase activity to cleave the covalent bond linking the polyketide's C1 carbon and the catalytic cysteine. In CHS, this bond is severed during the C6→C1 Claisen condensation reaction, but this same C1 thioester bond is not cleaved by STS's C2→C7 aldol condensation reaction. Although the STS reaction pathway clearly requires a thioesterase step, no such thioesterase-promoting residues in STS have been identified or even proposed prior to this study. It should be noted that the kinetics associated with thioesterase activity in the multifunctional STS active site cavity must be properly balanced relative to polyketide initiation and chain elongation, lest these preceding steps be derailed by premature liberation of thioester-linked polyketide intermediates from the catalytic cysteine.

The crystallographically observed thioesterase-like configuration of residues in both STS and the 18xCHS mutant led us to hypothesize that the mechanistic effects of these observed changes in region A are not steric, but rather mediated through the emergent STS hydrogen bonding network. To test this novel hypothesis, we introduced subtle point mutations intended to disrupt this hydrogen bonding system in the 18xCHS mutant (a functional stilbene synthase), while intentionally preserving the STS-like conformational changes we had already introduced into alfalfa CHS. As predicted for electronic rather than steric control of aldol cyclization specificity, each of these 18x(+1) CHS mutants (T132A, S131A, and E192Q) exhibited increased chalcone production at the expense of stilbene production (Figure 3E). (Residue 131 is neither solvent exposed nor displaced by the area 2 "kink," but its buried side chain hydroxyl also forms a hydrogen bond to the Glu192 side chain carboxylate.) While the E192Q mutation unfortunately causes enzyme instability (glutamate 192 is apparently also needed for fold stability, as it is absolutely conserved among type III PKS enzymes), this mutant's cyclization specificity follows a CHS-like C6→C1 Claisen condensation path. Conversely, the S131A and T132A 18x(+1) CHS mutants are relatively active and stable, and produce chalcone and resveratrol in ratios of roughly 50:50 and 75:25, respectively. Given the nature and position of the 18x(+1) CHS T132A and S131A mutations, and considering the fold instability of other mutant enzymes with fewer conformation-changing region A mutations than those comprising the (1210) 8xCHS mutant, the effect of these additional mutations is almost certainly electronic rather than steric. These results strongly indicate that STS aldol cyclization specificity is electronically mediated. Furthermore, aldol cyclization specificity is directly related to the observed thioesterase-like hydrogen bonding network connecting Glu192, through the repositioned Thr132 side chain hydroxyl, to a water molecule poised next to the catalytic cysteine. Consequently, we have labeled the STS-like rearrangement of these residues the "aldol switch."

Notably, the varying ratios of Claisen versus aldol cy-

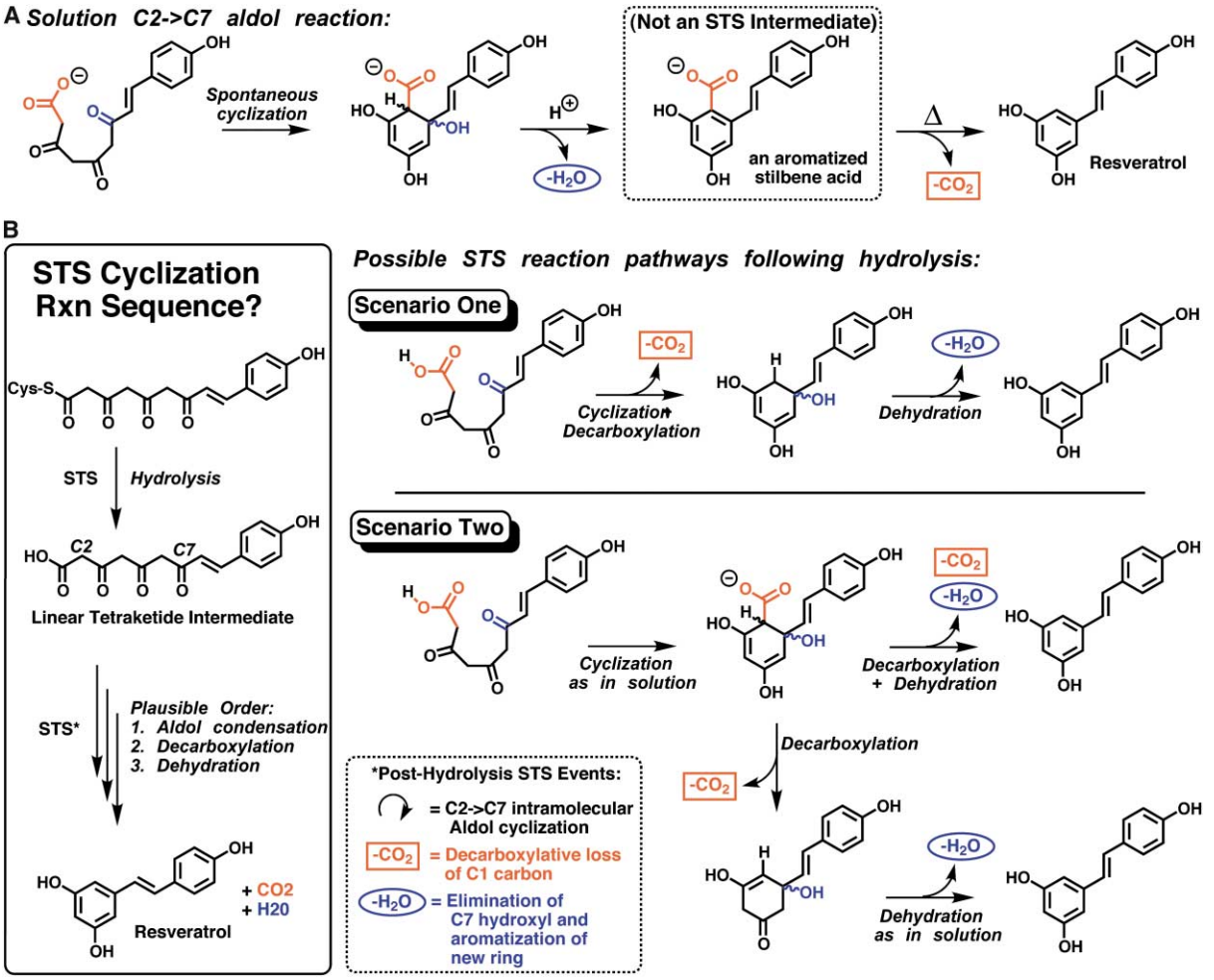


Figure 4. STS Mechanistic Options and Relevant Solution Chemistry

(A) Spontaneous solution-based polyketide C2→C7 aldol condensation cyclization chemistry leading to stilbenes. Atoms fated for elimination as molecules of $CO_2$ and $H_2O$ are colored in red and blue, respectively. The aromatized stilbene acid solution-based intermediate product has been shown not to be an intermediate in the STS-catalyzed reaction (see text).

(B) Plausible reaction pathways for the four STS cyclization-related events, assuming mechanistic divergence from CHS begins with an aldol switch-catalyzed thioesterase-like hydrolytic step. Scenario One depicts a decarboxylative cyclization reaction, as described by Ebizuka's group [14]. Scenario Two depicts two alternative decarboxylation schemes that follow a solution chemistry-like nondecarboxylative aldol condensation-based cyclization. Atoms fated for elimination as molecules of $CO_2$ and $H_2O$ are again colored red and blue, respectively.

clization specificity achieved with our 18x(+1) CHS T132A and S131A mutants represents a significant technological advance with implications for various PKS engineering projects, as it confirms that we can subtly manipulate the type III PKS aldol switch region to direct the biosynthesis of desired mixtures of chalcone and stilbene natural products emanating from a single mutant enzyme (for example, in any plant species' native CHS enzyme, already optimized by natural selection for expression in the cellular environment of that particular species). Thus, engineering the aldol switch provides a new biotechnological tool for optimizing resveratrol production to confer antifungal and nutritional value in engineered plants without abrogating the essential production of chalcone-derived flavonoids.

Interestingly, the eight pine STS-derived mutations that mechanistically convert alfalfa CHS to a stilbene synthase are not conserved residues in the STS enzymes from peanut or grapevine, confirming the lack of a universal STS consensus sequence. The only conserved trend across these eight scattered residues in diverse STSs is the substitution of a bulkier residue in place of CHS's Val98. However, we have quite recently solved the crystal structures of the peanut and grapevine STS enzymes, and our preliminary analysis of these STS enzymes demonstrates a conserved set of conformational changes in the aldol switch region, suggesting a conserved STS mechanism despite this sequence variation. A more comprehensive functional and structural analysis of the these peanut and grapevine STS aldol switch residues is underway and will be published with these additional STS crystal structures in the near future.

### Toward an Overall Mechanism for the Multistep Stilbene Synthase Reaction

As early as 1966, polyketide cyclization experiments carried out in solution by Harris and others revealed that both Claisen and aldol intramolecular cyclization

specificities were readily achievable using aqueous conditions over a range of pHs [19–22]. These elegant and informative biomimetic studies found that the cyclization fate of linear polyketides is mediated in solution by the presence or absence of an ester bond at the C1 carboxylate. More specifically, when C1 is part of an ester (or thioester) bond, C6→C1 Claisen cyclization predominates, while C2→C7 aldol cyclization is favored when C1 exists as a free acid (Figure 4A). These early findings foreshadow the most likely mechanistic interpretation of our current structural and mutagenic results. In contrast to more recent proposals that have assumed a steric mechanism of STS functional divergence from CHS, our findings suggest that the cyclization fate of the cysteine-linked tetraketide intermediate is determined by which of two competing processes occurs first in the type III PKS active site cavity: cleavage of the C1-cysteine thioester bond by a CHS-like intramolecular C6→C1 Claisen condensation, or hydrolysis of the same C1-cysteine thioester bond by an adjacent activated nucleophilic water molecule to form a free carboxylic acid intermediate. This acidic intermediate can then undergo facile aldol cyclization in the active site. In other words, the kinetic balance between Claisen-mediated ring cyclization and thioesterase-catalyzed hydrolysis of the tetraketide intermediate results in partitioning between parallel mechanistic pathways. This latter process is upregulated in stilbene synthases by the emergence of a thioesterase-like "aldol switch" hydrogen bonding network that allows Glu192, through Thr132, to activate a Ser338-positioned water molecule to a nucleophilic hydroxide anion for hydrolysis through base catalysis.

From an evolutionary standpoint, obtaining an alternative cyclization fate by promoting thioester hydrolysis to exploit intrinsic chemical reactivity is much simpler than having to precisely reposition an identical tetraketide intermediate in an alternate productive conformation using steric reshaping of the type III PKS active site cavity. Our current mechanistic proposal involving kinetic partitioning between competing pathways is also consistent with the observation that wild-type CHS and wild-type STS each produce minor amounts (1%–5%) of each other's major reaction product in vitro [23, 24].

Although our elucidation of the structural and functional basis for STS enzymes' divergent aldol cyclization specificity represents a significant achievement, as of yet we do not fully understand the complete STS reaction mechanism. Five distinct reaction events accompany STS's transformation of the linear tetraketide intermediate into a stilbene scaffold: (1) hydrolytic cleavage of the C1 thioester bond to the catalytic cysteine, (2) C2→C7 intramolecular aldol cyclization, (3) decarboxylative loss of C1 as $CO_2$, (4) dehydrative elimination of the tertiary alcohol derived from the C7 carbonyl oxygen, and (5) aromatization of the new stilbene ring (Figure 4B). Since equilibrium favors the enol form of the C3 and C5 carbonyls, only the tetrahedral sp3 hybridization of the predecarboxyled C2 and predehydrated C7 prevents immediate postcyclization aromatization. For our purposes, it is convenient to consider C7 dehydration and ring aromatization as a single event, reducing the number of variables from five to four. There are at least eight mechanistically plausible ways to order these four events, only four of which begin, as our current results suggest, with hydrolysis of the C1 thioester bond.

Previously, the discovery of stilbenecarboxylic acid natural products (stilbenes retaining the C1 carboxylate at the C2 position) in a few plants (but notably not pine, peanut, or grape) fostered the parsimonious assumption that stilbenecarboxylic acids must be on-pathway intermediates in stilbene biosynthesis (i.e., that STS-catalyzed aldol cyclization precedes C1 decarboxylation) [13], like the solution chemistry reaction sequence depicted in Figure 4A. Two recent pieces of evidence from Ebizuka's group call into question this mechanistic assumption [14]. First, a careful analysis of in vitro STS reaction products revealed absolutely no stilbenecarboxylic acid byproducts. Second, a deuterium-labeling experiment established that stilbene decarboxylation precedes aromatization of the new ring. These factors, along with the observation that CHS is more likely than STS to produce lactone derailment products, prompted Ebizuka's group to conclude that the STS mechanism likely initiates by hydrolysis of the linear tetraketide's C1 thioester linkage to cysteine, followed by a decarboxylative aldol cyclization [14], as shown in Scenario One of Figure 4B.

The idea that aldol cyclization could be driven by an energetically favorable elimination of C1 as a molecule of $CO_2$ is an appealing one. However, two lines of evidence from the early literature on biomimetic polyketide cyclization in solution suggest otherwise [19–22]. First, these studies indicate that C1 decarboxylation of linear polyketides competes with, rather than facilitates, the C2→C7 aldol cyclization of polyketides in solution. Furthermore, these experiments also show that decarboxylation does not accompany aldol cyclization in solution, but can be thermally induced afterwards (Figure 4A). Since aldol cyclization of polyketides in solution does not require energetic coupling to decarboxylation, it follows that there should be no energetic need to couple STS's enzymatic aldol cyclization reaction to decarboxylation, as implied by Scenario One.

Rather, our current structural and mutagenic results, when considered in light of solution-based polyketide aldol cyclization studies, imply that the STS active site is more likely to utilize a nondecarboxylative aldol cyclization, as depicted in Scenario Two of Figure 4B. However, the recent results from the Ebizuka group dictate that any STS mechanistic proposal that contains such a nondecarboxylative cyclization must also include a plausible mechanism for decarboxylating the resulting cyclized intermediate prior to ring aromatization. Logically, loss of the C1 carboxyl as $CO_2$ could either occur prior to, or in conjunction with, the dehydrative elimination of the C7 hydroxyl group (Figure 4B). In fact, there are plausible mechanistic options for both of these hypothetical postcyclization decarboxylation reaction pathways, which we will examine in greater detail below.

Beginning with a nondecarboxylative aldol cyclization, both Scenario Two options utilize shielding (by the exclusion of bulk solvent from the STS active site) to prevent the acid-catalyzed C7 dehydration reaction that produces aromatic stilbene acids in solution, as shown in Figure 4A, and instead employ intramolecular cyclic decarboxylation reactions as the next step after cyclization. Presumably, active site shielding might also favor

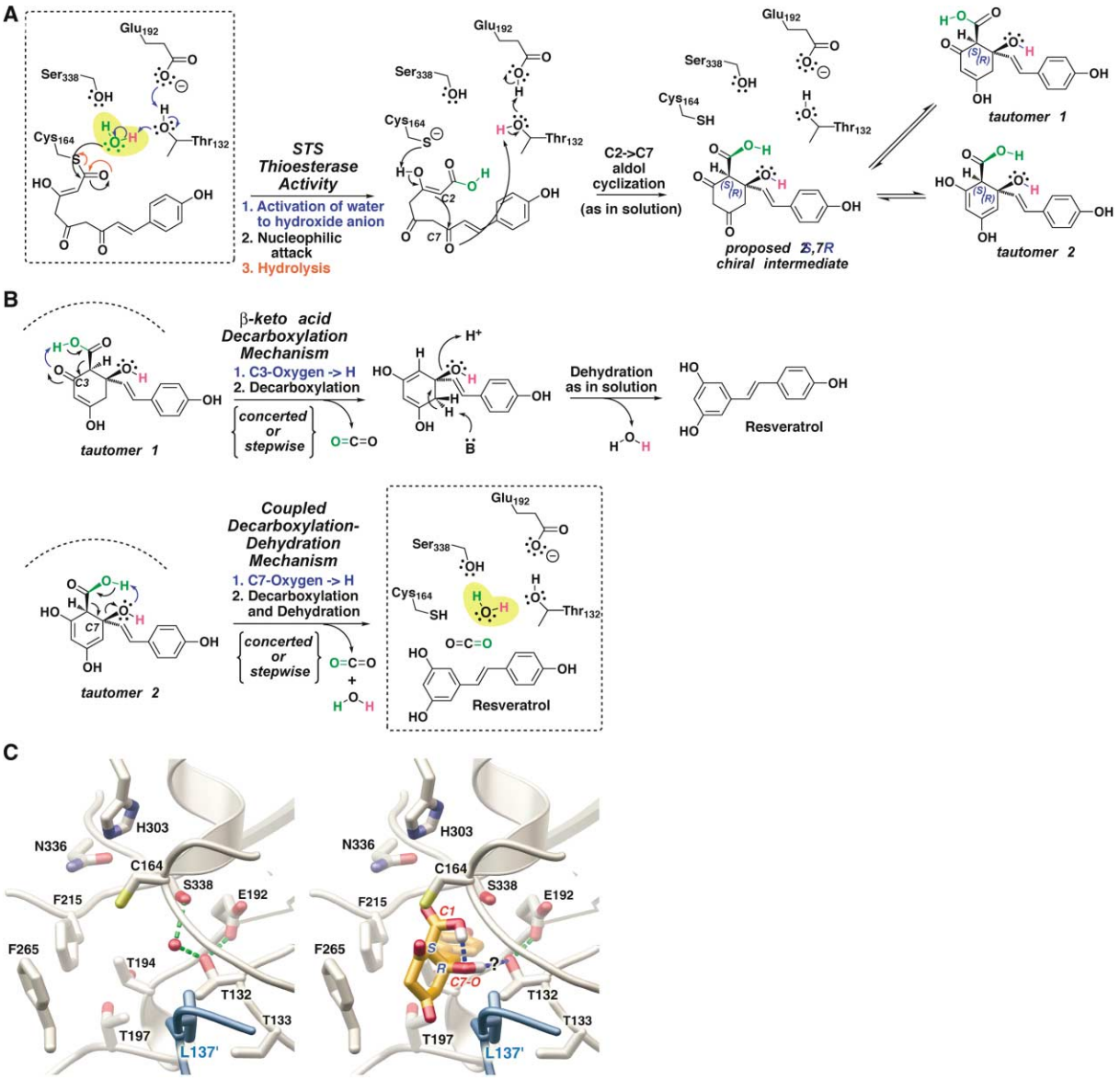


Figure 5. Detailed Alternative STS Mechanistic Proposals

(A) Detailed mechanism for our proposed thioesterase-like aldol switch hydrolysis step and subsequent solution-like nondecarboxylative aldol cyclization. The putative hydrolytic water molecule is highlighted in yellow, and its atoms are colored red or green, to track their movement and ultimate fates. Two enol tautomers of the proposed *2S,7R* chiral intermediate are shown, as they are relevant to the alternative decarboxylation mechanisms presented in (B).

(B) Two plausible alternative decarboxylation mechanisms (see text) involving intramolecular pericyclic electron movement (concerted or stepwise), proceeding from alternative enol tautomers of the cyclized intermediate shown in (A). Both decarboxylation alternatives require the enzymatic prevention of water-catalyzed dehydration leading to aromatized stilbene acids. Atom color denotes atoms derived from the catalytic water molecule shown in (A). The coupled decarboxylation-dehydration mechanism proceeding from tautomer two returns the aldol switch region to its precyclization state (dashed box, compare to [A], dashed box).

(C) The proposed chiral intermediate modeled in the STS-like 18xCHS active site cavity (second panel), in comparison to the observed positions of the putative hydrolytic water molecule and aldol switch residues (first panel). The position of the modeled chiral intermediate is based upon the positions of observed resveratrol complexes and modeled precyclization polyketide intermediates. Observed hydrogen bonds are in green, and putative hydrogen bonds involving the modeled intermediate are rendered in blue. Preservation of the C7 hydroxyl bond to Thr132 following cyclization requires a sterically permitted 30° rotation of the Thr132 side chain relative to its crystallographically observed depicted position. The modeled intermediate's chiral C2 and C7 positions are labeled with their predicted stereochemistry, and relevant protons on the C1 carboxyl and C7 hydroxyl group are rendered in white, with their modeled orientation corresponding to that depicted for tautomer 2 (see [A] and [B]).

these intramolecular decarboxylation mechanisms over externally catalyzed alternatives. In contrast to Scenario One's arbitrary decarboxylative C2→C7 cyclization mechanism, both Scenario Two mechanistic options utilize proven solution chemistry where appropriate and depart from solution chemistry in ways that make sense in the context of the enclosed STS active site cavity.

These more plausible mechanistic proposals embod-

ied in Scenario Two are further elaborated in Figure 5. Following thioester hydrolysis by the aldol switch-activated water molecule, the protonation of the C7 carbonyl oxygen that accompanies the STS-mediated aldol cyclization step may very well be catalyzed by the presence of the same aldol switch hydrogen bonding network, thus returning the aldol switch residues to their active form through indirect abstraction (mediated by Thr132) of the acidic proton on Glu192's protonated carboxyl group (Figure 5A).

Like all polyketides, this cyclized intermediate is capable of achieving several different combinations of keto-enol tautomers. In Figure 5B, each intramolecular decarboxylation reaction is depicted as proceeding from the tautomeric form of the cyclized polyketide that would seem to most favor that reaction. Both alternative decarboxylation reactions can exploit a six-center transition state arising from the intramolecular movement of three electron pairs. Our depiction here of cyclic intramolecular electron movement as concerted is not an assertion of simultaneous electron movement. Rather, we merely intend to convey that these six-centered intramolecular reactions have the potential to occur simultaneously, bypassing the production of high-energy polar intermediates [25].

One Scenario Two intramolecular decarboxylation option, suggested to us by a colleague (G. Weiss, personal communication), mirrors the concerted, six-center decarboxylation reaction of linear β-keto acids [26, 27] (Figure 5B). In this mechanistic scenario, the C3-derived carbonyl oxygen both abstracts the acidic proton from the C1 carboxyl moiety and also acts as an electron sink for decarboxylation of the C1 carboxyl group. Following this intramolecular reaction, a distinct acid-catalyzed protonation of the C7 hydroxyl group would be required to initiate C7 dehydration, presumably accompanied by aromatization of the stilbene's new resorcinol ring. Since STS does not produce stilbene acid derailment products, any such STS-catalyzed dehydration activity would need to scrupulously discriminate between the initial carboxyl-bearing and subsequently decarboxylated cyclized intermediates. Moreover, it is not obvious from inspection of the STS structure what active site feature would catalyze this dehydration function. Dehydration of this putative decarboxylated intermediate to produce the lower energy aromatic stilbene scaffold of resveratrol seems more likely to occur in solution, following diffusion out of the STS active site cavity. Presumably, the thermal C2 decarboxylation of C7-dehydrated stilbene acids in solution (Figure 4A) proceeds by a mechanism similar to this first proposal for C2 decarboxylation by STS.

The other plausible Scenario Two intramolecular decarboxylation mechanism, inspired by three-dimensional modeling of intermediates in the STS active site, utilizes a similar intramolecular cyclic transition state at the C2 carboxyl position, but one which involves an interaction with the C7 hydroxyl moiety rather than the C3 carbonyl group (Figure 5B, coupled decarboxylation/dehydration option). This alternative six-center reaction immediately achieves the lower energy aromatic stilbene scaffold of resveratrol by coupling C1 decarboxylation, intramolecular acid-catalyzed C7 hydroxyl loss, and aromatization of the stilbene ring, bypassing the competing linear β-ketoacid-like decarboxylation mechanism's need for an additional and intermolecular acid-catalyzed dehydration step.

Following the preceding cyclization step's putative proton transfer from Thr132 to the C7 oxygen moiety (Figure 5A), the position of the resulting C7 tertiary hydroxyl proton next to Thr132 in turn facilitates a hydrogen bond between a lone pair of electrons on the C7 hydroxyl oxygen and the C1 carboxyl's acidic proton. This geometry favors the formation of a cyclic, intramolecular six-membered transition state that simultaneously promotes proton transfer from the C1 carboxylic acid to the C7 hydroxyl, elimination of these respective ring substituents as molecules of $CO_2$ and $H_2O$, and formation of a double bond between C2 and C7.

While our proposed dehydrative decarboxylation mechanism has not been described to date, this intramolecular elimination ($E_i$) mechanism closely resembles a number of documented mechanistic precedents, although in solution this elimination mechanism usually requires thermal energy to achieve the relatively unfavorable *cis*-periplanar conformation necessary for the reaction [28–31]. In fact, these intramolecular elimination reactions most often occur in molecules where sigma bond rotation to achieve the lower energy *anti*-periplanar alternative productive conformation is sterically prevented by bulky substituents or by incorporation in ring systems [25]. In relation to the STS mechanism, we earlier stated that shielding in the active site cavity likely prevents the competing C7 dehydration reaction that produces stilbene acids following solution-based aldol cyclization reactions. This blocked dehydration reaction undoubtedly proceeds in solution via the lower energy *anti*-periplanar elimination of the remaining C2 proton. Although the documented $E_i$ reaction precedents employ seemingly more suitable leaving groups than the C7 tertiary alcohol depicted here, the combination of the very favorable intramolecular acid-catalyzed protonation of this tertiary alcohol and the aromatization of the resveratrol product may serve to make the resulting water molecule an equally favorable leaving group.

While these alternative Scenario Two intramolecular decarboxylation mechanistic proposals require very similar catalytic requirements from the STS active site (i.e., shielding), they differ in their stereochemical requirements. Although the aromatic stilbene product is achiral, the initial cyclized intermediate produced by a nondecarboxylative aldol condensation possesses two chiral carbons (C2 and C7). While the β-ketoacid decarboxylation proposal is consistent with any of these stereoisomers, the coupled decarboxylation-dehydration proposal requires the initial cyclized intermediate to have a *cis* arrangement of its C7 hydroxyl and C1 carboxyl groups, and thus is consistent with only two stereoisomers (2*S*, 7*R* or 2*R*, 7*S*). Significantly, this *cis* juxtaposition of the C7 hydroxyl group and the C1 carboxyl moiety, which allows the C1 free acid's acidic proton to catalyze the intramolecular dehydration of the C7 hydroxyl, is energetically favored in these two stereoisomers because of the favorable orientation of the C1 carboxyl on C2 *trans* to C7's other substituent (the much larger starter-derived coumaroyl moiety).

Based upon the three-dimensional modeling of both linear and cyclized intermediates in the STS active site

cavity, we predict that the initial cyclized intermediate resulting from a nondecarboxylative C2→C7 aldol cyclization in the STS active site cavity is most likely to possess 2*S*, 7*R* stereochemistry. Figure 4C models this predicted intermediate in the STS active site cavity. The position shown is based on the observed position and orientation of bound resveratrol (Figure 3A), the location of the putative hydrolytic water molecule, and the modeled positions and orientations of precyclization tetraketide intermediates.

The putative 2*S*, 7*R* stereochemistry of the cyclized intermediate represents the first stereochemical prediction of a transitory chiral STS reaction intermediate. Although this stereochemistry is compatible with both of our postcyclization intramolecular decarboxylation mechanistic proposals, our structure-based prediction of this cyclized intermediate's stereochemistry may facilitate the design of potential STS reaction intermediate analogs or inhibitors that can be used to distinguish one decarboxylation mechanism over the other. Similarly, a very recent analysis found the catalytic cysteines of CHS and STS enzymes to differ significantly from each other in their susceptibility to inhibition by various chloroacetamide herbicides [32]. This result was unexpected, as the relative susceptibility of condensing enzymes to particular inhibitors most often correlates with differences in their active site volumes. In retrospect, the different responses of CHS and STS enzymes to these chloroacetamide herbicides may be mediated by the aldol switch region differences we report here, given the close proximity of the catalytic cysteine and the aldol switch region.

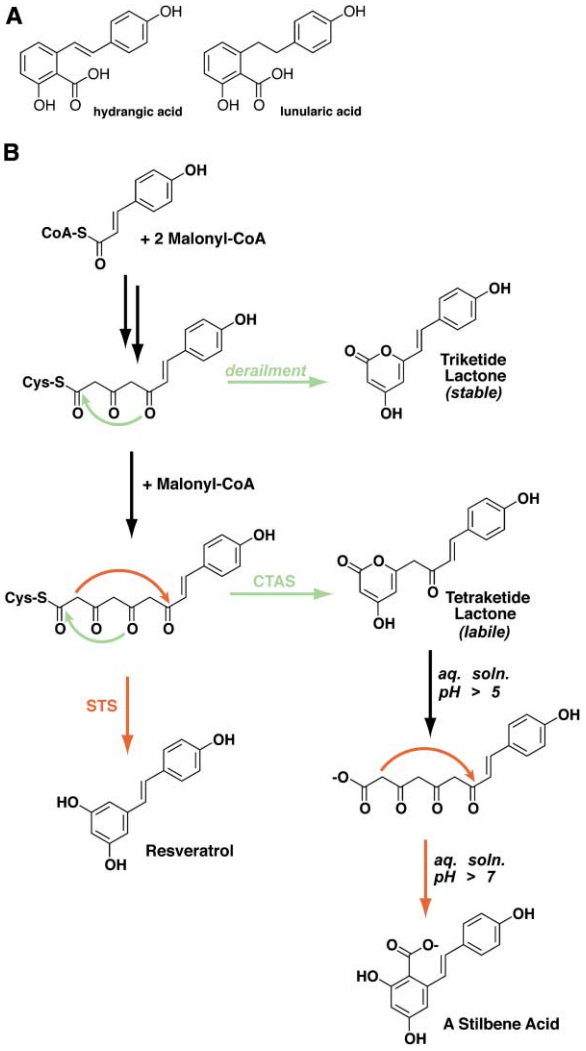


Figure 6. Stilbenecarboxylic Acid Biosynthetic Proposal

(A) Biological stilbene acids discussed in the text (hydrangic and lunularic acids). Note missing hydroxyls (compared to generic stilbene acid in Figure 1D or in [B]) indicating reduction of a polyketide intermediate.

(B) Novel proposal for stilbene acid biosynthesis based upon solution chemistry (see Figure 4A and text) and observed product specificities of CTAS enzymes (see text). O5→C1 lactonization reactions are shown in green, with C2→C7 aldol condensations shown in red.

### Insights into Stilbenecarboxylic Acid Biosynthesis

It is fitting to conclude this analysis with some structural and mechanistic insights into the related topic of stilbenecarboxylate (also known as stilbenecarboxylic acid or stilbene acid) biosynthesis. Like stilbenes, these rare natural products have been isolated from a small but diverse collection of plants, including species of *Hydrangea* and primitive liverworts of the *Marchantia* family [2]. Labeling experiments and the incorporation of stilbenecarboxylates into well-characterized downstream natural products demonstrate that the isolation of in vivo stilbene acids is neither an artifact nor a by-product of stilbene biosynthesis [14]. These natural products presumably result via a nondecarboxylative STS-like (C2→C7 aldol) type III PKS reaction mechanism. The same reaction pathway, but proceeding from an aliphatic hexanoyl starter, is likely to be responsible for the carboxylate-bearing resorcinol moiety of tetrahydrocannabinol (THC) compounds in *Cannabis*. While candidate type III PKS enzymes have been cloned from some species, in vitro reconstitution of stilbenecarboxylate biosynthesis has been problematic at best.

Two independent attempts to clone and characterize stilbenecarboxylic acid synthases have been published, with each group finding only one candidate (i.e., non-CHS) type III PKS enzyme [33, 34]. Ebizuka's group, searching for *Hydrangea macrophylla* var. *thunbergii*'s hydrangic acid (Figure 6A) synthase, cloned an enzyme that in vitro efficiently produced *p*-coumaroyltriacetic acid lactone (CTAL), a minor tetraketide CHS derailment product, from *p*-coumaroyl-CoA and three molecules of malonyl-CoA [33]. This enzyme was named *p*-coumaroyltriacetic acid synthase (CTAS) (Figures 1D and 6B). Schröder's group independently observed the same lactone product specificity with the only apparent non-CHS type III PKS in *Hydrangea macrophylla* L. (Garden Hortensia), a species containing both hydrangic acid and the similar lunularic acid (Figure 6A) [34]. However, when primed with dihydro-*p*-coumaroyl-CoA as a starter, this enzyme produced nearly 50% 5-hydroxylunularic acid, a stilbenecarboxylic acid, in addition to triketide and tetraketide lactones. Notably, this group also detected 5-hydroxylunularic acid when a pine CHS was given the dihydro-*p*-coumaroyl-CoA starter, while a pine

STS given the same starter failed to produce a stilbenecarboxylic acid. These results are extremely puzzling if one assumes stilbenes and stilbenecarboxylates are produced by a conserved biosynthetic mechanism.

Both publications discussed plausible explanations for these expected stilbenecarboxylate synthases' surprising in vitro activities, including the influence of a missing polyketide ketoreduction step (reviewed in [2]) indicated by the hydroxylation pattern of the *Hydrangea* stilbenecarboxylates (see Figure 6). Schröder's group noted that ketoreduction of the C5 polyketide position or use of the dihydro-*p*-coumaroyl starter both interrupt the extensive $\pi$ bond conjugation system possible in the unreduced *p*-coumaroyl-derived tetraketide intermediate [34].

However, now that the structural basis for STS-like aldol cyclization specificity has been elucidated, it is clear that the *Hydrangea* CTAS sequences contain no such STS-like signatures and are in fact quite CHS-like aside from one important (but non-STS-like) T197N active site substitution. Notably, CHS enzymes produce more in vitro lactone derailment products than do STS enzymes, even when provided with their physiological starters [23]. Although lactone derailment products are often assumed to form in solution after hydrolytic release of linear free acid polyketide intermediates, our current study of STS suggests hydrolysis in the STS active site cavity leads to the production of stilbenes. It therefore seems likely that lactone formation initiates CTAS-like product off-loading via an intramolecular attack by the C5 keto-enol oxygen on the cysteine-tethered C1 thioester. Similar to CHS's C6→C1 cyclization and product release, and distinct from STS's water-mediated thioester hydrolysis, the C1-tethered tetraketide conformation leading to CTAL is likely favored by the position 197 substitution. Significantly, a T197L point mutant of the well-characterized alfalfa CHS was previously shown to mirror CTAS's fairly exclusive production of CTAL [16].

The biomimetic polyketide cyclization literature dating back to the late 1960's reveals several pieces of circumstantial evidence that together suggest a new interpretation of both the in vitro activity of CTAS enzymes and the in vivo production of stilbenecarboxylates that has not been addressed in the CTAS literature. These studies suggest that the cloned *Hydrangea* CTAS enzymes are in fact responsible for the in vivo biosynthesis of the stilbenecarboxylic acid precursor CTAL. Most notably, in solution the labile CTAL lactone can precede the spontaneous aldol condensation leading to stilbenecarboxylic acids. We propose that the final aldol cyclization step is not catalyzed by a type III PKS at all, and is likely to have emerged in *Hydrangea* and other stilbenecarboxylate-producing species as the natural consequence of forming tetraketide lactones at physiological pH. Significantly, the standard assays employed in the published CTAS studies would prevent detection of all but the most facile solution-phase aldol cyclizations. It is also possible that some unidentified enzyme may subsequently have been recruited to catalyze this spontaneous but slow process.

While free $\beta$-keto carboxylic acids (i.e., linear polyketides) readily form lactones in acidic solution, solution studies demonstrate that they undergo spontaneous aldol cyclization when placed in basic or mildly acidic conditions [19–22]. Furthermore, while triketide lactones are quite stable in solution, tetraketide lactones, over time, are much more likely to reopen, and in neutral or basic solution, the resulting linear free acid is likely to undergo C2→C7 aldol cyclization rather than relactonization [20]. Thus, even if the observed *Hydrangea* PKS lactones form in the active site, the tetraketide-derived CTAL is considerably less stable in solution than is the triketide-derived bis-noryangonin, and thus much more likely under physiological conditions to reopen and subsequently undergo spontaneous aldol cyclization to form a stilbenecarboxylate. Unlike STS's type III PKS-catalyzed aldol cyclization, nonenzymatic C2→C7 aldol cyclizations are almost never accompanied by spontaneous decarboxylation, overwhelmingly producing stilbenecarboxylates as their stable end products. In fact, the decarboxylation of stilbenecarboxylates in solution requires considerable thermal energy [22].

Consistent with the Schröder group's results, the nature of the R group attached to a linear tetraketide also modulates its rate of spontaneous aldol cyclization. In the linear tetraketide intermediates formed by type III PKS enzymes, this R group represents the entire starter molecule-derived portion except for the C7 ketone (see R′ in Figure 1C). While a methyl R group facilitates very rapid solution aldol cyclization, other substituents promote slower processes, especially those containing a $\pi$ bond conjugated with the C7 ketone [22, 35], such as in *p*-coumaroyl-derived (but not dihydro-*p*-coumaroyl-derived) tetraketides. Notably, all of the *Hydrangea* PKS in vitro assays were extracted after 30–60 minutes [33, 34], which is too short of a time frame to allow for most spontaneous aldol cyclizations to occur [22, 35]. In light of these facts, the supposedly enzymatic in vitro formation of stilbenecarboxylates only from a dihydro-*p*-coumaroyl-CoA starter, especially when associated with high yields of tri- and tetraketide lactones [34], is more likely to result from spontaneous solution aldol cyclization of a linear tetraketide (reopened lactone). Given a longer reaction time before acid quenching, the *p*-coumaroyl-initiated CTAS reaction would likely also result in the spontaneous and very favorable production of stilbenecarboxylates.

## Significance

**Chalcone synthase (CHS) and stilbene synthase (STS) are related type III polyketide synthase (PKS) enzymes that catalyze the formation of identical linear tetraketide intermediates. However, each catalyzes the cyclization of this reactive polyketide intermediate using alternative intramolecular condensation mechanisms. CHS, ubiquitous in the plant kingdom, catalyzes a C6→C1 Claisen condensation to form the core chalcone scaffold of all flavonoid natural products. Conversely, STS has evolved in a limited number of phylogenetically distinct plants via gene duplication and subsequent mechanistic divergence from CHS, and instead catalyzes a C2→C7 aldol condensation that forms the stilbene backbone of resveratrol and related**

**antifungal phytoalexins. Stilbenes can confer antifungal resistance to host plants when STS is heterologously expressed in them, and as phytonutrients in mammalian diets, they also possess a number of health benefits for humans and other animals. Here we present the first STS crystal structure and the detailed structural comparison to previously characterized CHS that guided our subsequent mutagenic conversion of alfalfa CHS into a functional STS. Significantly, we identify the previously obscure structural basis for the evolution of STSs from their CHS ancestors. Unexpectedly, the mechanism of STS functional divergence stems from the emergence of a cryptic thioesterase activity in the active site, due to an alternative hydrogen bonding network termed the "aldol switch." This mechanism is distinct from previous models of type III PKS functional divergence that imply that steric factors that shape the active site cavity thereby direct the conformation and thus the cyclization fate of polyketide intermediates. Finally, we propose a novel mechanistic hypothesis, derived from existing biomimetic polyketide cyclization studies, that explains a series of puzzling experimental results in the related field of stilbenecarboxylic acid biosynthesis. The discovery of the structural basis of stilbene biosynthesis fills a major gap in our understanding of the structural and mechanistic underpinnings of functional diversity in the type III PKS enzyme superfamily, as aldol condensation-driven polyketide cyclization was one of the least understood type III PKS reactions. The successful structurally guided engineering of efficient STS activity into CHS demonstrates the utility of this combined structure-function approach in numerous type III PKS engineering projects.**

## Experimental Procedures

### Mutagenesis

Single or a minimal set of multiple site mutations in contiguous areas of primary sequence were introduced using the QuikChange system (Stratagene). More extensive mutations in each area were generated using a second round of QuickChange with new mutagenic primers and a CHS gene template already mutated to the "intermediate" sequence shown in Figure 2C. Mutagenesis at multiple distal sites was achieved by PCR amplification of wild-type (or "intermediate" mutant) regions using 5′ and 3′ primers containing mutagenic changes. Following purification using agarose gel electrophoresis, these overlapping fragments were assembled and amplified by PCR with the appropriate end primers to generate contiguous mutant megaprimers that spanned several distal sites and contained all of the desired mutations. These megaprimers were then separately incorporated into the full-length alfalfa CHS gene (in the pHIS-8 expression vector construct [36]) by the QuickChange method. Each mutation was confirmed by automated nucleotide sequencing (Salk Institute DNA sequencing facility).

### Protein Expression and Purification

*P. sylvestris* STS was subcloned into the pHIS-8 expression vector, as previously described for *M. sativa* CHS2 [36]. Following overexpression in *E. coli* BL21(DE3) cells, recombinant proteins were purified to homogeneity, concentrated to between 5 and 50 mg/ml, and stored at −80°C following buffer exchange into 12 mM HEPES (pH 7.5), 25 mM NaCl, and 5 mM DTT, as described previously [36].

### Crystallization and Data Collection

*P. sylvestris* STS and the 18xCHS mutant were crystallized by vapor diffusion in hanging drops consisting of a 1:1 mixture of protein and crystallization buffer, in the presence of 1 mm DTT. The wild-type STS crystallization buffer contained 13% (w/v) PEG 8000, 300 mM ammonium acetate, and 100 mM $MOPSO^{-}Na^{+}$ buffer at pH 7.0. Prior to freezing in liquid nitrogen, STS crystals were equilibrated for 2 min in a cryogenic buffer identical to the crystallization buffer except for the use of 15% (w/v) PEG 8000 and the inclusion of 10% (v/v) glycerol, and then moved into a similar solution containing 25% (v/v) glycerol for another 2 min. The apo 18xCHS crystallization buffer contained 21% (w/v) PEG 8000, 300 mM ammonium acetate, 100 mM $HEPES^{-}Na^{+}$ buffer at pH 7.5, and 3% (v/v) ethylene glycol, whereas the 18xCHS resveratrol complex crystal was obtained by the inclusion of 2.5 mM *trans*-resveratrol in the 18xCHS crystallization buffer. Prior to freezing, both the apo and resveratrol-complexed 18xCHS crystals were subjected to a 60 s cryogenic soak in crystallization buffer modified to contain 23% (w/v) PEG 8000 and 6% (v/v) ethylene glycol.

*P. sylvestris* STS crystallized in the $P2_1$ space group, with unit cell dimensions of a = 57.2 Å, b = 361.3 Å, c = 57.3 Å, $\alpha = \gamma = 90.0°$, and $\beta = 98.4°$, and six monomers (three physiological homodimers) in the asymmetric unit. The apo 18xCHS crystals also grew in the $P2_1$ space group, but with a much smaller unit cell of a = 71.6 Å, b = 59.8 Å, c = 82.5 Å, $\alpha = \gamma = 90.0°$, and $\beta = 108.2°$, with only two monomers (one homodimer) in the asymmetric unit. Conversely, the 18xCHS resveratrol complex crystallized in the P1 space group, with unit cell dimensions of a = 64.3 Å, b = 71.7 Å, c = 85.7 Å, $\alpha = 111.4°$, $\beta = 91.6°$, and $\gamma = 90.1°$, and four monomers (two dimers) in the unit cell (asymmetric unit).

Data were collected at the Stanford Synchrotron Radiation Laboratory (SSRL) or at the European Synchrotron Radiation Facility (ESRF). Diffraction images were indexed and integrated with DENZO [37], the reflections were merged with SCALEPACK [37], and data reduction was completed with CCP4 programs [38] or using XDS [39]. Despite strong diffraction, overlapping reflections caused by one unusually long STS unit cell axis (b = 361.3 Å) seriously complicated this particular data collection. Although the application of an additional spacial deconvolution step carried out using PROW [40] improved completeness (without increasing the $R_{sym}$), many problematic overlapping reflections remained, resulting in only 74% completeness and less than ideal crystallographic statistics (see Table 1).

### Structure Determination and Refinement

All structures were solved by molecular replacement using EPMR [41] or AMoRe [42]. For both the wild-type STS and the apo 18xCHS structures, the search model consisted of a homology model based upon the alfalfa CHS2 crystal structure, generated with MODELLER [43]. The refined apo 18xCHS structural model was used as the search model for the 18xCHS resveratrol complex.

Solutions were iteratively refined using CNS [44] or REFMAC [45]. Inspection of the $|2F_o - F_c|$ and $|F_o - F_c|$ electron density maps and model building were performed in O [46]. The final refinement statistics for each structure are listed in Table 1. Each residue's backbone conformation was categorized (by CCP4's PROCHECK analysis of Ramachandran plots [38]) as either core (most favorable), allowed, generally allowed, or disallowed. The percentage of the final pine STS model's residues in each group is 87.9%, 11.2%, 0.8%, and 0.05%, respectively. The corresponding values for the 18xCHS apo structure's residues are 90.3%, 8.8%, 0.75%, and 0.15%, while the results with the resveratrol-complexed 18xCHS structure's residues are 90.5%, 9.2%, 0.3%, and 0.075%. Each structure had only one residue (of only one monomer) in a disallowed conformation, in each case a glutamine (position 234 in STS, 231 in CHS) involved in a hairpin turn at the protein surface (distant from the active site). Notably, a similar backbone conformation of Gln231 was observed in the previously reported wild-type CHS structure [12].

Structural illustrations were prepared with MOLSCRIPT [47] and were rendered with POV-Ray [48].

### Enzyme Assays and Determination of Kinetic Constants

Mutant CHS enzyme assays were conducted as detailed elsewhere [36], in this case side-by-side with both wild-type CHS and wild-type STS enzymes, all utilizing *p*-coumaroyl-CoA and [2-$C^{14}$]-malonyl-CoA substrates and including a final reaction mixture acidifica-

tion step to maximize detection of any potential lactone derailment products. Radiolabeled products were extracted, separated by TLC as described prevously [36], and then visualized with film or with a Molecular Dynamics PhosphorImager system. Product ratios were quantified using Molecular Dynamics ImageQuant software.

Steady-state kinetic constants were determined from linear initial velocity measurements utilizing radiolabeled malonyl-CoA, Ecolume scintillation fluid, and a scintillation counter, as detailed previously [36].

**Acknowledgments**

M.B.A. thanks J. Jez for introduction to type III PKS radiochemical assays, kinetics, and crystallographic methods. We thank B. Moore, M. Burkhart, and G. Weiss for helpful mechanistic discussions. This material is based upon work supported by the National Science Foundation under Grant No. 0236027 to J.P.N. Portions of this research were carried out at the Stanford Synchrotron Radiation Laboratory, a national user facility operated by Stanford University on behalf of the U.S. Department of Energy, Office of Basic Energy Sciences. The SSRL Structural Molecular Biology Program is supported by the Department of Energy, Office of Biological and Environmental Research, and by the National Institutes of Health, National Center for Research Resources, Biomedical Technology Program. We also acknowledge the European Synchrotron Radiation Facility for provision of synchrotron radiation facilities. The technology associated with this manuscript has been licensed through the Salk Institute to Allylix, Inc. The corresponding author (J.P.N.) is a cofounder of Allylix, Inc.

Received: February 26, 2004
Revised: May 6, 2004
Accepted: May 19, 2004
Published: September 17, 2004

**References**

1. Schröder, J. (2000). The family of chalcone synthase-related proteins: functional diversity and evolution. Recent Adv. Phytochem. *34*, 55–89.
2. Austin, M.B., and Noel, J.P. (2003). The chalcone synthase superfamily of type III polyketide synthases. Nat. Prod. Rep. *20*, 79–110.
3. Schröder, J., and Schröder, G. (1990). Stilbene and chalcone synthases: related enzymes with key functions in plant-specific pathways. Z. Naturforsch. [C] *45*, 1–8.
4. Tropf, S., Lanz, T., Rensing, S.A., Schröder, J., and Schröder, G. (1994). Evidence that stilbene synthases have developed from chalcone synthases several times in the course of evolution. J. Mol. Evol. *38*, 610–618.
5. Hain, R., Reif, H.J., Krause, E., Langebartels, R., Kindl, H., Vornam, B., Wiese, W., Schmelzer, E., Schreier, P.H., Stocker, R.H., et al. (1993). Disease resistance results from foreign phytoalexin expression in a novel plant. Nature *361*, 153–156.
6. Hipskind, J.D., and Paiva, N.L. (2000). Constitutive accumulation of a resveratrol-glucoside in transgenic alfalfa increases resistance to Phoma medicaginis. Mol. Plant Microbe Interact. *13*, 551–562.
7. Siemann, E.H., and Creasy, L.L. (1992). Concentration of phytoalexin resveratrol in wine. Am J Enol Vitic. *43*, 49–52.
8. Soleas, G.J., Diamandis, E.P., and Goldberg, D.M. (1997). Resveratrol: a molecule whose time has come? And gone? Clin. Biochem. *30*, 91–113.
9. Fremont, L. (2000). Biological effects of resveratrol. Life Sci. *66*, 663–673.
10. Howitz, K.T., Bitterman, K.J., Cohen, H.Y., Lamming, D.W., Lavu, S., Wood, J.G., Zipkin, R.E., Chung, P., Kisielewski, A., Zhang, L.L., et al. (2003). Small molecule activators of sirtuins extend *Saccharomyces cerevisiae* lifespan. Nature *425*, 191–196.
11. Tropf, S., Kärcher, B., Schröder, G., and Schröder, J. (1995). Reaction mechanisms of homodimeric plant polyketide synthase (stilbenes and chalcone synthase). A single active site for the condensing reaction is sufficient for synthesis of stilbenes, chalcones, and 6′-deoxychalcones. J. Biol. Chem. *270*, 7922–7928.
12. Ferrer, J.L., Jez, J.M., Bowman, M.E., Dixon, R.A., and Noel, J.P. (1999). Structure of chalcone synthase and the molecular basis of plant polyketide biosynthesis. Nat. Struct. Biol. *6*, 775–784.
13. Schröder, J. (1997). A family of plant-specific polyketide synthases: facts and predictictions. Trends Plant Sci. *2*, 373–378.
14. Shibuya, M., Nishioka, M., Sankawa, U., and Ebizuka, Y. (2002). Incorporation of three deuterium atoms excludes intermediacy of stilbenecarboxylic acid in stilbene synthase reaction. Tetrahedron Lett. *43*, 5071–5074.
15. Schanz, S., Schröder, G., and Schröder, J. (1992). Stilbene synthase from Scots pine (Pinus sylvestris). FEBS Lett. *313*, 71–74.
16. Jez, J.M., Austin, M.B., Ferrer, J., Bowman, M.E., Schröder, J., and Noel, J.P. (2000). Structural control of polyketide formation in plant-specific polyketide synthases. Chem. Biol. *7*, 919–930.
17. Schröder, J. (1999). The chalcone/stilbene synthase-type family of condensing enzymes. In Comprehensive Natural Reports, D. Barton, K. Nakanishi, O. Meth-Cohn, and U. Sankawa. eds. (Oxford, UK: Elsevier). pp. 749–772.
18. Li, J., Derewenda, U., Dauter, Z., Smith, S., and Derewenda, Z.S. (2000). Crystal structure of the *Escherichia coli* thioesterase II, a homolog of the human Nef binding enzyme. Nat. Struct. Biol. *7*, 555–559.
19. Harris, T.M., and Carney, R.L. (1966). Biogenetically modeled synthesis of β-resorcylic acids. J. Am. Chem. Soc. *88*, 2053–2054.
20. Bentley, R., and Zwitkowits, P.M. (1967). Biosynthesis of tropolones in *Penicillium stipitatum*. VII. The formation of polyketide lactones and other nontropolone compounds as a result of ethionine inhibition. J. Am. Chem. Soc. *89*, 676–680.
21. Harris, T.M., and Carney, R.L. (1967). Synthesis of 3,5,7-triketo acids and esters and their cyclizations to resorcinol and phloroglucinol derivatives. Models of biosynthesis of phenolic compounds. J. Am. Chem. Soc. *89*, 6734–6741.
22. Harris, T.M., and Harris, C.M. (1986). Biomimetic syntheses of aromatic polyketide metabolites. Pure Appl. Chem. *58*, 283–294.
23. Yamaguchi, T., Kurosaki, F., Suh, D.Y., Sankawa, U., Nishioka, M., Akiyama, T., Shibuya, M., and Ebizuka, Y. (1999). Cross-reaction of chalcone synthase and stilbene synthase overexpressed in Escherichia coli. FEBS Lett. *460*, 457–461.
24. Suh, D.Y., Kagami, J., Fukuma, K., Iwanami, N., Yamazaki, Y., Yurimoto, H., Sakai, Y., Kato, N., Shibuya, M., Ebizuka, Y., et al. (2000). Chalcone and stilbene synthases expressed in eucaryotes exhibit reduced cross-reactivity in vitro. Chem. Pharm. Bull. (Tokyo) *48*, 1051–1054.
25. Carey, F.A., and Sundberg, R.J. (1990). Advanced Organic Chemistry. Part B: Reactions and Synthesis. Third Edition (New York: Plenum Press).
26. Jencks, W.P. (1969). Catalysis in Chemistry and Enzymology. (New York: McGraw-Hill).
27. Westheimer, F.H., and Jones, W.A. (1941). The effect of solvent on some reaction rates. J. Am. Chem. Soc. *63*, 3283–3286.
28. Cope, A.C., and Trumbull, E.R. (1960). Olefins from amines: the Hofmann elimination reaction and amine oxide pyrolysis. Org. React. *11*, 317–493.
29. Clive, D.L.J. (1978). Modern organoselenium chemistry. Tetrahedron *34*, 1049–1132.
30. DePuy, C.H., and King, R.W. (1960). Pyrolytic cis eliminations. Chem. Rev. *60*, 431–457.
31. Nace, H.R. (1962). The preparation of olefins by the pyrolysis of xanthates. The Chugaev reaction. Org. React. *12*, 57–100.
32. Eckermann, C., Matthes, B., Nimtz, M., Reiser, B., Lederer, B., Böger, P., and Schroder, J. (2003). Covalent binding of chloroacetamide herbicides to the active site cysteine of plant type III polyketide synthases. Phytochemistry *64*, 1045–1054.
33. Akiyama, T., Shibuya, M., Liu, H.M., and Ebizuka, Y. (1999). p-Coumaroyltriacetic acid synthase, a new homologue of chalcone synthase, from Hydrangea macrophylla var. thunbergii. Eur. J. Biochem. *263*, 834–839.
34. Eckermann, C., Schroder, G., Eckermann, S., Strack, D., Schmidt, J., Schneider, B., and Schroder, J. (2003). Stilbenecar-

boxylate biosynthesis: a new function in the family of chalcone synthase-related proteins. Phytochemistry *62*, 271–286.
35. Howarth, T.T., Murphy, G.P., and Harris, T.M. (1969). Preparation and biogenetic-type aromatizations of tetraacetic acid (3,5,7-trioxooctanoic acid). J. Am. Chem. Soc. *91*, 517–518.
36. Jez, J.M., Ferrer, J.L., Bowman, M.E., Dixon, R.A., and Noel, J.P. (2000). Dissection of malonyl-coenzyme A decarboxylation from polyketide formation in the reaction mechanism of a plant polyketide synthase. Biochemistry *39*, 890–902.
37. Otwinowski, Z., and Minor, W. (1997). Processing of X-ray diffraction data collected in oscillation mode. Methods Enzymol. *276*, 307–326.
38. Dodson, E.J., Winn, M., and Ralph, A. (1997). Collaborative Computational Project, Number 4: providing programs for protein crystallography. Methods Enzymol. *277*, 620–633.
39. Kabsch, W. (1993). Automatic processing of rotation diffraction data from crystals of initially unknown symmetry and cell constants. J. Appl. Crystallogr. *26*, 795–800.
40. Bourgeois, D., Nurizzo, D., Kahn, R., and Cambillau, C. (1998). An integration routine based on profile fitting with optimized fitting area for the evaluation of weak and/or overlapped two-dimensional laue or monochromatic patterns. J. Appl. Crystallogr. *31*, 22–35.
41. Kissinger, C.R., Gehlaar, D.K., and Fogel, D.B. (1999). Rapid automated molecular replacement by evolutionary search. Acta Crystallogr. D Biol. Crystallogr. *55*, 484–491.
42. Navaza, J. (2001). Implementation of molecular replacement in AMoRe. Acta Crystallogr. D Biol. Crystallogr. *57*, 1367–1372.
43. Sali, A., and Blundell, T.L. (1993). Comparative protein modeling by satisfaction of spatial restraints. J. Mol. Biol. *234*, 779–815.
44. Brunger, A.T., Adams, P.D., Clore, G.M., DeLano, W.L., Gros, P., Grosse-Kunstleve, R.W., Jiang, J.S., Kuszewski, J., Nilges, M., Pannu, N.S., et al. (1998). Crystallography and NMR system: a new software suite for macromolecular structure determination. Acta Crystallogr. D Biol. Crystallogr. *54*, 905–921.
45. Murshudov, G.N., Vagin, A.A., and Dodson, E.J. (1997). Refinement of macromolecular structures by the maximum-likelihood method. Acta Crystallogr. D Biol. Crystallogr. *53*, 240–255.
46. Jones, T.A., Zou, J.Y., Cowan, S.W., and Kjeldgaard, M. (1993). Improved methods for building protein models in electron density maps and the location of errors in these models. Acta Crystallogr. D Biol. Crystallogr. *49*, 148–157.
47. Kraulis, P.J. (1991). MOLSCRIPT: a program to produce both detailed and schematic plots of protein structures. J. Appl. Crystallogr. *24*, 946–950.
48. POV-Team. (1997). POV-Ray: persistence of vision ray-tracer. (http://www.povray.org).

**Accession Numbers**

Coordinates and structure factors for each structure have been deposited in the Protein Data Bank (pine STS [1U0U], 18xCHS mutant [1U0V], and 18xCHS/resveratrol complex [1U0W]).